SEMARAK ILMU PUBLISHING

Semarak Engineering Journal

Journal homepage:
https://semarakilmu.my/index.php/sej/index
ISSN: 3036-0145

Numerical Analysis of Heat and Mass Transmission for Micropolar Nanofluid Flow over an Inclined Surface with Soret-Dufour Effects

Gamal R. Elkahlout[1,*]

[1] School of Business Studies, Arab Open University, Riyadh, Saudi Arabia

ARTICLE INFO

Article history:
Received 3 June 2025
Received in revised form 5 January 2026
Accepted 8 March 2026
Available online 3 April 2026

Keywords:
Micropolar nanofluid; Stagnation flow; Soret and Dufour effects; Keller-Box Technique

ABSTRACT

Nanofluids exhibiting high heat transmission ability are vibrant in modern-day industrial applications. As a result, scientists are always working to create more efficient mechanisms, efficient energy systems etc. Therefore a mathematical model with physical assumptions has been formulated in order to examine the energy and mass transport characteristics in a micropolar nanofluid flow. The purpose of this study is to examine the energy and mass transfer phenomenon of micropolar nanofluid flow over an exponentially stretching surface by incorporating Soret and Dufour effects. It utilizes a model based on the Buongiorno model, incorporating the effects of Brownian motion and thermophoretic forces. By introducing suitable similarity variables, the flow modeled equations are into a set of nonlinear ordinary differential equations. Numerical solutions of this flow model are obtained using the Keller box method, a reliable and widely employed approach for solving nonlinear boundary value problems. Results show that, as the radiation parameter increases, the heat transfer rate of the fluid increases, while the energy transfer rate decreases. Additionally, it is observed that the increment in Dufour effect increases the temperature distribution. Moreover, skin-friction coefficient increases with the inclination factor, whereas energy and mass transmission rate decrease.

1. Introduction

Nanofluid term refers to the suspension of solid nanoparticles such as silver, copper, titanium dioxide, or aluminum oxide in a base fluid like water, oil, or glycol. The thermal conductivity of regular base fluids is increased by adding metallic nanometer-sized particles to the base fluids. Nanofluid thermal efficiency can be predicted to be higher than that of the base fluids. Such fluids can be used in the cooling of nuclear reactors, electronic devices, vehicles, cancer therapy, and the heating and cooling of energy conversion processes.

In experimental research introduced by Choi *et al.*, [1], it was discovered that adding nanoparticles can improve the thermal conductivity of the base fluids. Buongiorno [2] discovered the convective transport phenomena in nanofluid flow and constructed a mathematical model to study

* *Corresponding author.*
E-mail address: g.elkahlout@arabou.edu.sa

https://doi.org/10.37934/sej.13.1.156167

the performance of nanoparticles in a nanofluid flow, including the influences of Brownian motion and thermophoretic dispersion.

Numerical and experimental analyses of nanofluid flow were investigated by Alhajaj et al. [3]. Recently, Najib *et al.,* [4] performed stability analysis for the nanoliquid by considering a shrinking and extendable cylinder. Furthermore, Najid *et al.,* [5] considered the nanoliquid for examining the second slip impacts on extendable/ contracting surfaces via stability analysis. Anuar *et al.* [6] probed the stagnation flow of a hybrid nanoliquid for an exponentially stretchy surface. They incorporated suction and injection impacts into their study. Studies by several authors [7-12] illustrate some recent investigations into nanofluid flows.

Numerous engineering applications utilize the boundary layer flow through a stretching sheet, including reducing drag, improving grain storage, minimizing skin friction, and enhancing paper manufacture. Sakiadis [13] conducted the first investigation on boundary layer flow across a continuous solid surface with constant velocity. The effect of an electric field on the MHD flow of nanoliquid to a nonlinear extended surface with variable thickness was explored by Daniel *et al.,* [14].

Complex partial differential equations are reduced to dimensional ordinary differential equations by suitable similarity transformations, and an implicit finite difference scheme is used to solve them. When the electric field decreases, the concentration, velocity, and temperature of the nanofluid are increased.

Numerical modeling of boundary layer flow with electrically conductive nanofluid over a sheet of variable thickness, subjected to nonlinear stretching, was examined by Daniel et al. [15]. The stagnation point flow of a heated porous stretching sheet past a radiative magneto micropolar liquid was numerically investigated by Warke *et al.*, [16]. Current research on the flow past a stretching sheet is mentioned by several authors [17-24].

Soret and Dufour impacts were analyzed by Hayat *et al.*, [25] in the second-grade fluid's magnetohydrodynamic three-dimensional flow. Moreover, Najib and Bachok [26] examined the Soret and Dufour effects via stability analysis to check the behavior of energy and mass transfer for a moving surface.

In order to account for thermal radiation, Soret effects, and Dufour effects, the energy and concentration equations were modeled. Sardar et al. [27] researched on the mixed convection flow of Carreau nanofluid over a wedge when Soret and Dufour effects were present. The effects of Soret and Dufour on heat and mass transfer in a salt gradient solar pond were examined quantitatively by Khan *et al.,* [28].

The nonlinear radiative flow between two stretchable impermeable rotating discs was studied by Qayyum *et al.,* [29]. The Soret and Dufour effects were also used. Anwar *et al.,* [30] and Rafique [31] studied the impact of Soret and Dufour factors on the flow of nanoliquid over a porous surface. Soret and Dufour effects were considered during the modeling of energy expression. For numerical solutions, they used the Keller box approach.

In view of the earlier literature there is no study available which discuss the Soret and Dufour effects on micropolar nanofluid flow over an exponentially stretching surface numerically via Keller box technique. In order to fill this gap, with a focus on micropolar nanofluid flow current research has been conducted. It consists on multiple complex phenomena including Soret and Dufour effects, Stagnation point flow, Inclination effect, Brownian motion and thermophoresis impacts in a single frame work. This investigation of various effects helps us to understand the flow behavior of fluid in various industrial and engineering applications including, paper production, heat exchangers and chemical reactors. Furthermore, the consideration of solutal and thermal expansions along with thermal radiations effects broaden the scope of this research to explore how these influences affect the flow dynamic. For the investigation of this article there are many numerical techniques, but we

chose Keller box scheme because it is easier to program, gives more accuracy and friendly use. Furthermore, we conducted this research to provide new perceptions and enhance the existing knowledge gap.

2. Materials and Methodology

In this article, we examined the micropolar nanoliquid flow above an exponentially stretchy surface. Further, for the analysis of energy and mass transfer, the impacts of Soret and Dufour are considered. Here, we consider both the stretching and free stream velocities as exponential functions, $u_w(x) = ae^{x/l}$ and $u \to u_\infty(x) = be^{x/l}$ where, a and b are constants, and x is the coordinate measured along the stretching sheet. The fluid base includes micropolar finite-sized particles that rotate, in addition to nanoparticles. At the wall boundary, the temperature T and nanoparticle fraction C remain constant, denoted by T_w and C_w respectively, representing the fixed thermal and concentration conditions at the wall. Furthermore, Figure 1 exhibits that as y approaches infinity, the ambient values are denoted by T_∞ and C_∞.

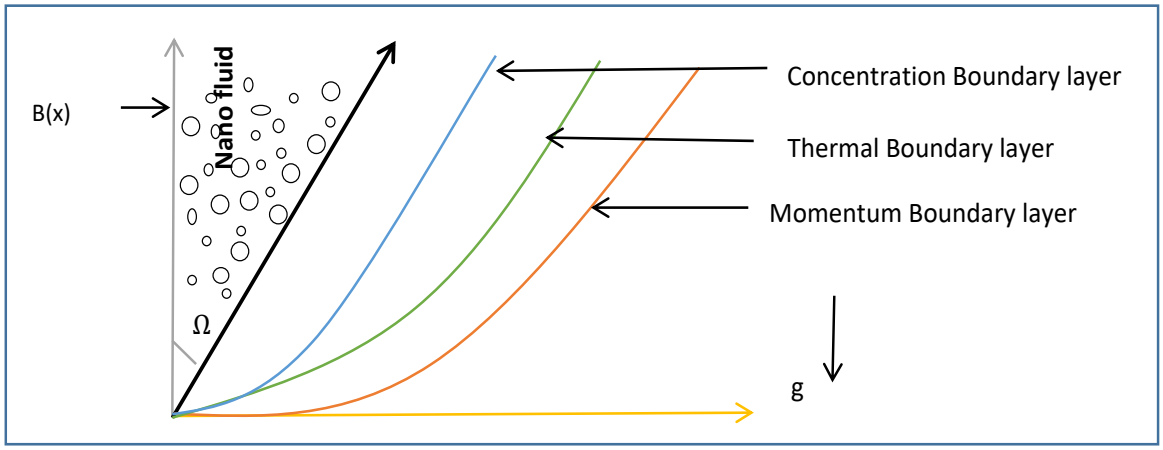

Fig. 1. Physical model and coordinate system

Equations that govern boundary layers, as viewed by several authors [32-34], are

$$\frac{\partial u}{\partial x} + \frac{\partial v}{\partial y} = 0, \tag{1}$$

$$u\frac{\partial u}{\partial x} + v\frac{\partial u}{\partial y} = u_\infty \frac{du_\infty}{dx} + \left(\frac{\mu + k_1^*}{\rho}\right)\frac{\partial^2 u}{\partial y^2} + \left(\frac{k_1^*}{\rho}\right)\frac{\partial N^*}{\partial x} + \frac{\sigma B^2}{\rho}(u_\infty - u) + g[\beta_t(T - T_\infty) + \beta_c(C - C_\infty)]Cos\gamma\,, \tag{2}$$

$$u\frac{\partial N^*}{\partial x} + v\frac{\partial N^*}{\partial y} = \left(\frac{\gamma^*}{j^*\rho}\right)\frac{\partial^2 N^*}{\partial y^2} - \left(\frac{k_1^*}{j^*\rho}\right)\left(2N^* + \frac{\partial u}{\partial y}\right), \tag{3}$$

$$u\frac{\partial T}{\partial x} + v\frac{\partial T}{\partial y} = \alpha\frac{\partial^2 T}{\partial y^2} - \frac{1}{(\rho c)_f}\frac{\partial q_r}{\partial y} + \tau\left[D_B\frac{\partial C}{\partial y}\frac{\partial T}{\partial y} + \frac{D_T}{T_\infty}\left(\frac{\partial T}{\partial y}\right)^2\right] + \frac{D_T K_T}{c_s c_p}\frac{\partial^2 C}{\partial y^2}, \tag{4}$$

$$u\frac{\partial C}{\partial x} + v\frac{\partial C}{\partial y} = D_B\frac{\partial^2 C}{\partial y^2} + \frac{D_T K_T}{T_\infty}\frac{\partial^2 T}{\partial y^2}. \tag{5}$$

Using the Rosseland approximation, Eq. (4) can be simplified and resulting in a reduced expression for the radiative heat flux, which is:

$$q_r = \frac{-4\sigma^*}{3k^*}\frac{\partial T^4}{\partial y}, \quad \text{and} \quad T^4 = 4T_\infty^3 T - 3T_\infty^4, \tag{6}$$

So Eq. (4)'s simplified form is

$$u\frac{\partial T}{\partial x} + v\frac{\partial T}{\partial y} = \alpha\left(1 + \frac{4N}{3}\right)\frac{\partial^2 T}{\partial y^2} + \tau\left[D_B\frac{\partial C}{\partial y}\frac{\partial T}{\partial y} + \frac{D_T}{T_\infty}\left(\frac{\partial T}{\partial y}\right)^2\right] \tag{7}$$

The following physical quantities and variables are used in this research:

• u and v: velocity components in *x* and *y* directions • ρ: density of base fluid • k_1^*: vertex viscosity • $\alpha = \frac{k}{(\rho c)_f}$: thermal diffusivity parameter, where *k* is the thermal conductivity, and $(\rho c)_f$ is the heat capacity of the base fluid. • $\tau = \frac{(\rho c)_p}{(\rho c)_f}$: ratio of heat capacity of nanoparticles to base fluid • σ: electrical conductivity	• μ: viscosity • $\gamma*$: viscosity of spin gradient • $j*$: micro-inertia per unit mass • N: radiation parameter • D_T: thermophoresis diffusion coefficient • D_B: Brownian motion coefficient • c_s: concentration susceptibility • c_p: specific heat • K_T: thermal diffusion ratio

The imposed boundary conditions are given below:

$$u = u_w(x) = ae^{x/l}, \ v = 0, \ N^* = -n_0\frac{\partial u}{\partial y}, \qquad T = T_w(x), \qquad C = C_w(x) \quad at \ (y = 0)$$

$$u \to u_\infty = be^{x/l}, \ v \to 0, \ N^* \to 0, \ T \to T_w, \ C \to C_w \quad \text{as} \quad y \to \infty. \tag{8}$$

When $n_0 = 0$ results in $N^* = 0$ at the wall, indicating a concentrated flow profile where the micro-elements of rotational motion are restricted near the wall surface. To convert the nonlinear partial differential equations into nonlinear ordinary differential equations, we utilize similar transformations, which are specified. Stream function $\sigma\psi = \psi(x, y)$ represented by:

$$u = \frac{\partial\psi}{\partial y}, v = -\frac{\partial\psi}{\partial x}. \tag{9}$$

The similarity transformations are defined using the exponentially stretching sheet's velocity in the following form:

$$\psi = \sqrt{2lva}e^{\frac{x}{2l}}f(\eta), \quad N^* = \left(\frac{a}{2vl}\right)e^{\frac{3x}{2l}}\sqrt{2lva}h(\eta), \quad \theta(\eta) = \frac{T-T_\infty}{T_w-T_\infty}, \quad \phi(\eta) = \frac{C-C_\infty}{C_w-C_\infty} \tag{10}$$

Where, $T_w = T_\infty + T_0e^{\frac{x}{2l}}$, $C_w = C_\infty + C_0e^{\frac{x}{2l}}$.

In simpler terms, when Eq. (10) is inserted into Eq. (2) to Eq. (7), it will be converted to the following nonlinear ordinary differential equations:

$$(1+K)f''' + ff'' - 2f'^2 + 2\gamma^2 + Kh' + M(\gamma - f') + (\lambda\theta + \delta\phi)Cos\Omega = 0, \quad (11)$$

$$\left(1+\frac{K}{2}\right)h'' + h'f - 3f'h - K(2h + f'') = 0, \quad (12)$$

$$\left(1+\frac{4}{3}N\right)\theta'' + (\theta' f - \theta f' + Nb\theta'\,\phi' + Nt\theta'^2)\Pr + (D_f\,\phi'')\Pr = 0, \quad (13)$$

$$\phi'' + Le(\phi' f - \phi f') + LeS_r\theta'' = 0, \quad (14)$$

Where,

$$\gamma = \frac{b}{a}, Pr = \frac{\nu}{\alpha}, Le = \frac{\nu}{D_B}, M = \frac{2l\sigma B_0^2}{a\rho}, K = \frac{k_1^*}{\mu}, Nb = \frac{D_B\tau(C_w - C_\infty)}{\nu}, Nt = \frac{\tau D_T(T_w - T_\infty)}{\nu T_\infty}, \lambda = \frac{G_r}{Re_x^2}, \delta = \frac{G_C}{Re_x^2},$$

$$G_r = \frac{2gB_t(T_w - T_\infty)l^3}{\nu^2}, G_c = \frac{2gB_c(C_w - C_\infty)l^3}{\nu^2}, D_f = \frac{D_m k_T(C_w - C_\infty)}{\nu c_s c_p(T_w - T_\infty)}, S_r = \frac{D_T k_T(T_w - T_\infty)}{\nu T_\infty(C_w - C_\infty)}, N = \frac{4\sigma T_\infty^3}{kk^*}, \quad (15)$$

Where prime notation represents derivatives with respect to η. M denotes Magnetic parameter which is known as the Hartmann number, Pr stands for Prandtl number, Le denotes Lewis number, Nt_b=$\frac{Nt}{Nb}$ where N_t is thermophoresis, and N_b is Brownian motion, λ denotes Parameter for buoyancy forces, S_r stands for Soret number and D_f denotes Dufour number.

The boundary conditions specified in Eq. (8) are transformed into:

$$f'(\eta) = 1, f(\eta) = 0,\ h(\eta) = -n_0 f''(\eta), \phi(\eta) = 1, \theta(\eta) = 1,\ at\ \eta = 0,$$

$$f'(\eta) \to \gamma, \theta(\eta) \to 0, h(\eta) \to 0, \phi(\eta) \to 0\ \ as\ \eta \to \infty. \quad (16)$$

The Sherwood number (Sh), skin friction coefficient (C_{fx}) and the Nusselt number (Nu), defined as follows:

$$Sh = \frac{xq_m}{D_B(C_w - C_\infty)}, \qquad Nu = \frac{xq_w}{k(T_w - T_\infty)}, \qquad C_{fx} = \frac{\tau_w}{\rho u_w^2}. \quad (17)$$

Where $\tau_w = (\mu + k_1^*)\frac{\partial u}{\partial y} + k_1^* N^*,\ q_w = -k\frac{\partial T}{\partial y}$ and $q_m = -D_B\frac{\partial C}{\partial y}\ at\ y = 0$ are the shear stress, energy flux, and. mass flux at the sheet, respectively.

The connection between the skin friction coefficient $C_{fx}(0) = (1+K)f''(0)$,. the reduced Sherwood. number $-\phi'(0)$ and the reduced Nusselt number. $-\theta'(0)$ are expressed as:

$$C_{fx}(0) = C_f\sqrt{Re_x}, -\phi'(0) = \frac{Sh}{\sqrt{Re_x}}, \quad -\theta'(0) = \frac{Nu}{(1-\frac{4}{3}N)\sqrt{Re_x}}. \quad (18)$$

Here, the local Reynolds number is $Re_x = \frac{axe^{x/l}}{\nu}$.

3. Results and Discussion

Here, we analyzed the numerical outcomes of transformed nonlinear ordinary differential equations from Eq. (11) to Eq. (14) under specified boundary conditions in Eq. (16), using the Keller-box method for explanation. The Keller-box approach is a computer-based mathematical method for solving boundary problems. It divides the problem into smaller sections and then takes steps to arrive at an approximate solution. Since it is accurate and fast in solving problems, it is widely used in science and engineering.

The numerical outcomes for the appropriate physical parameters are exhibited in tabular form in Tables 1 and 2, providing a clear and concise overview of the findings. The current results are compared to the existing outcomes of Ishak [31] and Bidin and Nazar [32]. Table 1 shows a high level of consistency observed between the findings.

Table 1
Evaluation of reduced Nusselt number $-\theta'(0)$ when $\delta, Nb, Nt, \lambda, K, Le, \gamma, S_r, D_f = 0$and $\Omega = 90^0$

Pr	M	N	Bidin & Nazar [33]	Ishak [32]	Present results
			$-\theta'(0)$	$-\theta'(0)$	$-\theta'(0)$
1.0	0	0	0.9548	0.9548	0.9548
2.0	0	0	1.4714	1.4714	1.4714
3.0	0	0	1.8691	1.8691	1.8691
1.0	0	1.0	0.5312	0.5312	0.5312
1.0	1.0	0	--	0.8611	0.8611
1.0	1.0	1.0	--	0.4505	0.4505

Table 2
Values of $-\theta'(0)$, $-\phi'(0)$ and $C_{fx}(0)$

Nb	Nt	Pr	Le	M	K	N	S_r	D_f	λ	δ	γ	Ω	$-\theta'(0)$	$-\phi'(0)$	$C_{fx}(0)$
0.1	0.1	6.5	5.0	0.1	1.0	1.0	0.1	0.1	0.1	0.1	0.5	45^0	0.3257	1.7579	0.8452
0.3	0.1	6.5	5.0	0.1	1.0	1.0	0.1	0.1	0.1	0.1	0.5	45^0	0.1231	1.8333	0.8435
0.1	**0.3**	6.5	5.0	0.1	1.0	1.0	0.1	0.1	0.1	0.1	0.5	45^0	0.1404	1.8164	0.8425
0.1	0.1	**9.0**	5.0	0.1	1.0	1.0	0.1	0.1	0.1	0.1	0.5	45^0	0.1382	1.8562	0.8468
0.1	0.1	6.5	**9.0**	0.1	1.0	1.0	0.1	0.1	0.1	0.1	0.5	45^0	-0.5131	3.2597	0.8490
0.1	0.1	6.5	5.0	**0.3**	1.0	1.0	0.1	0.1	0.1	0.1	0.5	45^0	0.3219	1.7514	0.9086
0.1	0.1	6.5	5.0	0.1	**3.0**	1.0	0.1	0.1	0.1	0.1	0.5	45^0	0.3392	1.7858	1.1116
0.1	0.1	6.5	5.0	0.1	1.0	**3.0**	0.1	0.1	0.1	0.1	0.5	45^0	-0.1003	1.8731	0.8349
0.1	0.1	6.5	5.0	0.1	1.0	1.0	**0.5**	0.1	0.1	0.1	0.5	45^0	1.0610	0.4176	0.8344
0.1	0.1	6.5	5.0	0.1	1.0	1.0	0.1	**0.3**	0.1	0.1	0.5	45^0	2.8577	-0.0262	0.8974
0.1	0.1	6.5	5.0	0.1	1.0	1.0	0.1	0.1	**0.3**	0.1	0.5	45^0	0.3285	1.7636	0.7741
0.1	0.1	6.5	5.0	0.1	1.0	1.0	0.1	0.1	0.1	**0.9**	0.5	45^0	0.3308	1.7696	0.6685
0.1	0.1	6.5	5.0	0.1	1.0	1.0	0.1	0.1	0.1	0.1	**0.7**	45^0	0.3473	1.7941	0.5351
0.1	0.1	6.5	5.0	0.1	1.0	1.0	0.1	0.1	0.1	0.1	0.5	$\mathbf{60^0}$	0.3251	1.7567	0.8622

The micropolar nanoliquid flow over an extending sheet is considered numerically via the Keller-box approach, and the results are displayed in various plots. Figure 1 shows a physical representation of the problem. The outcomes are computed for embedded parameters and displayed in Figures 2 to 12.

Figure 2 is plotted for the impact of the magnetic field *M* on velocity outlined for both $\gamma < 1$ and $\gamma > 1$. The data indicates that the dimensionless velocity profile $f'(\eta)$ is reduced for < 1 , but is enhanced for $\gamma > 1$ as the magnetic field intensity increases.

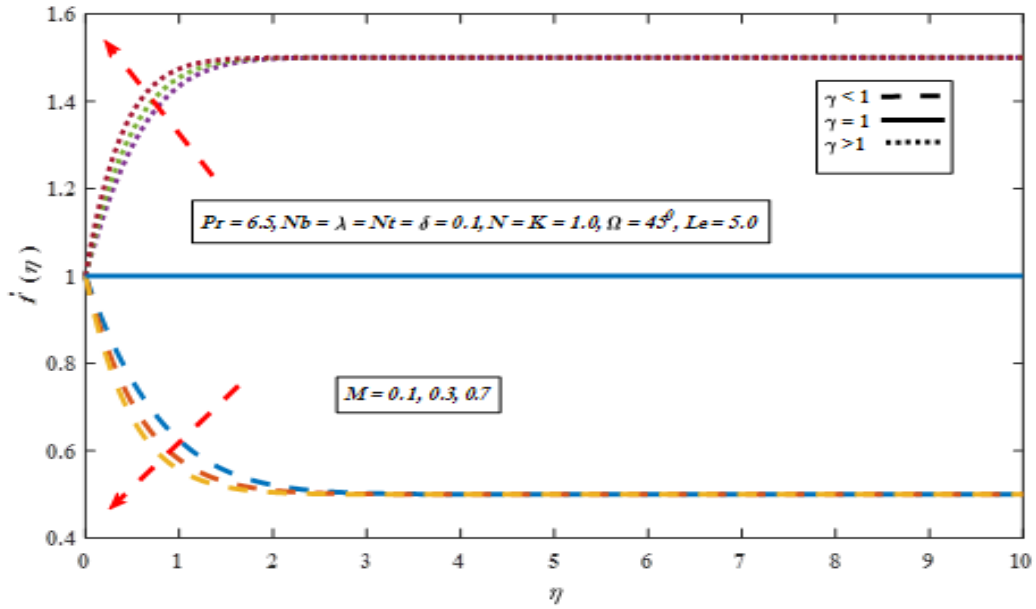

Fig. 2. Impacts of the Magnetic parameter *M* on $f'(\eta)$

Moreover, as shown in Figure 3, $f'(\eta)$ exhibits an enhancement with increasing γ applicable to both cases of $\gamma < 1$ and $\gamma > 1$. The flow improves the boundary layer when $\gamma > 1$, representing that the free stream velocity exceeds the stretchable velocity, producing a noticeable change in the flow's behavior. Physically, the liquid motion near the stagnation point becomes more pronounced, causing the external flow to accelerate more rapidly.

Consequently, the boundary layer thickness decreases as γ increases. Alternatively, a reverse boundary layer forms, while the stream's velocity is slower than the stretching velocity ($\gamma < 1$). When $\gamma = 1$, there is no boundary layer improvement and, the stream's velocity is equal to the stretching velocity.

An increase in the Prandtl number *Pr* is accompanied by a decrease in temperature and a reduction in boundary layer thickness, as shown in Figure 4, resulting in a thinner boundary layer. From a physical perspective, a larger *Pr* signifies that the fluid's momentum diffuses more easily than its heat, due to the greater momentum diffusivity relative to thermal diffusivity. The reduction in thermal diffusivity led to a decrease in temperature.

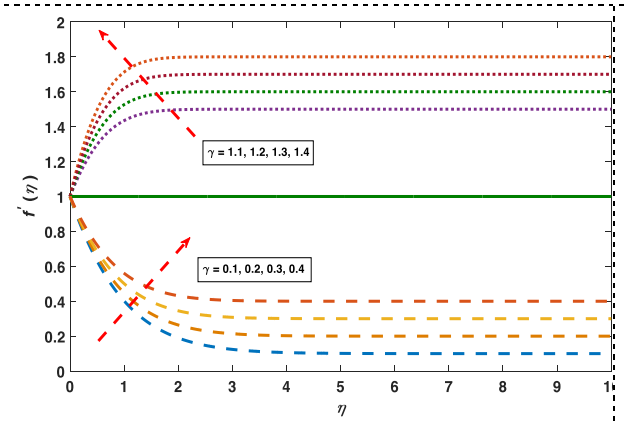

Fig. 3. Impacts of Velocity ratio parameter (γ) on $f'(\eta)$

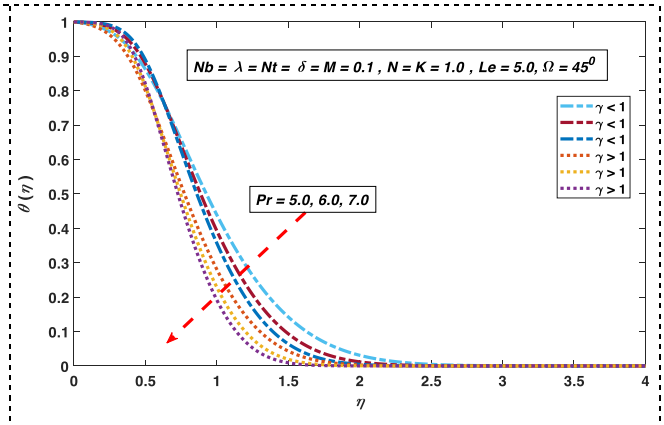

Fig. 4. Impacts of Prandtl number (Pr) on $\theta(\eta)$

Figure 5 is depicted to show how the Dufour number D_f affects the temperature profile. When we increase the values of the D_f, the temperature field is seen to behave in an increasing manner. The temperature profile's behavior is displayed in Figure 6, demonstrating the impact of thermal radiation *N* on the temperature distribution. Enhancement in radiation parameter indicates to rise in the temperature profile, resulting in heat being produced in the flow field and an increase in the thermal boundary layer's temperature.

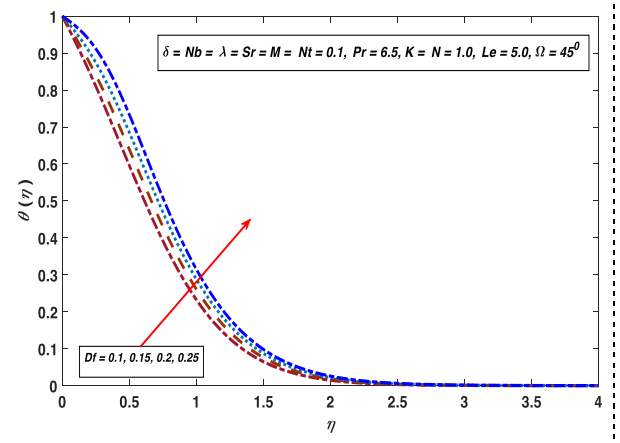

Fig. 5. Impacts of Dufour number on $\theta(\eta)$

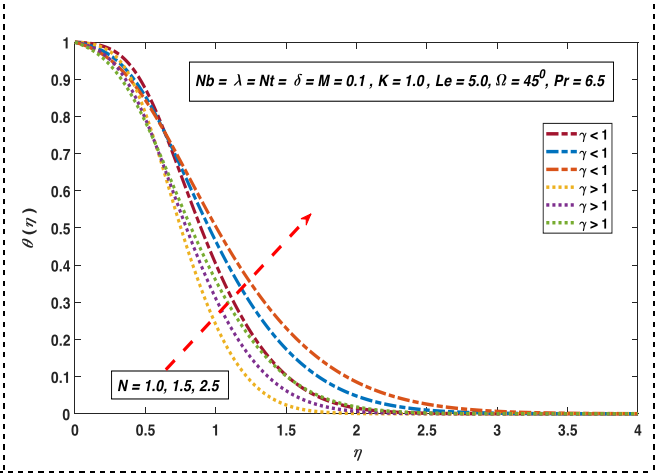

Fig. 6. Impacts of Radiation parameter (N) on (η)

Increases in Nb (Brownian motion) create irregular particle movement, which warms the boundary layer and raises the fluid temperature. The temperature profile gets higher in response to these boosts in Nb. The thermophoretic effects on the thermal profile in opposition to $\gamma < 1$ and $\gamma > 1$ are presented in Figure 8. The results of the thermophoresis display a clear association with the temperature field because changes in the wall and reference temperatures have a positive impact on the thermophoretic factor, resulting to a similar rise in the temperature profile.

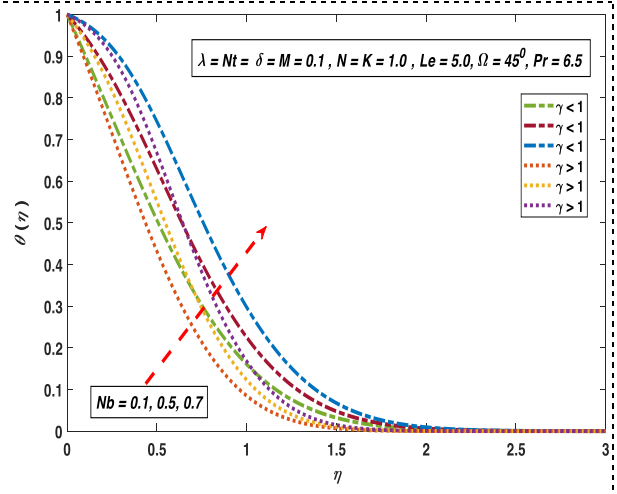

Fig. 7. Impacts of Brownian motion parameter *Nb* on $\theta(\eta)$

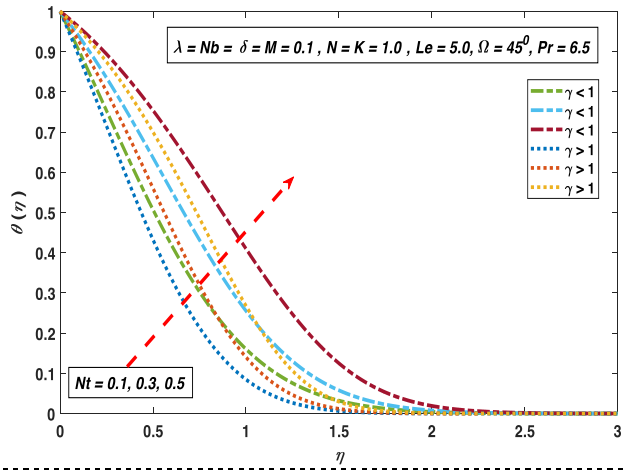

Fig. 8. Impacts of Thermophoresis parameter Nt on $\theta(\eta)$

Figure 9 is depicted to show how the Soret number (S_r) affects the concentration profile. It has been noted that for larger values of S_r, concentration profile is higher. Figure 10 displays impact of thermophoresis on concentration profile $\phi(\eta)$, considering both cases of $\gamma < 1$ and $\gamma > 1$. As shown in the figure, it is clear that the concentration decreases as the value of Nt changes.

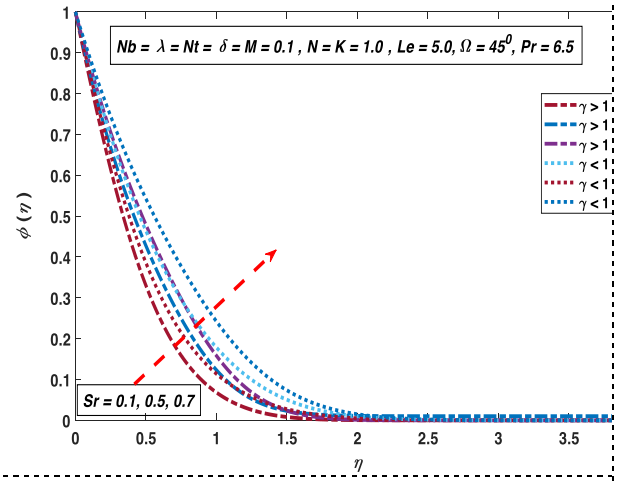

Fig. 9. Impacts of Soret number on $\phi(\eta)$

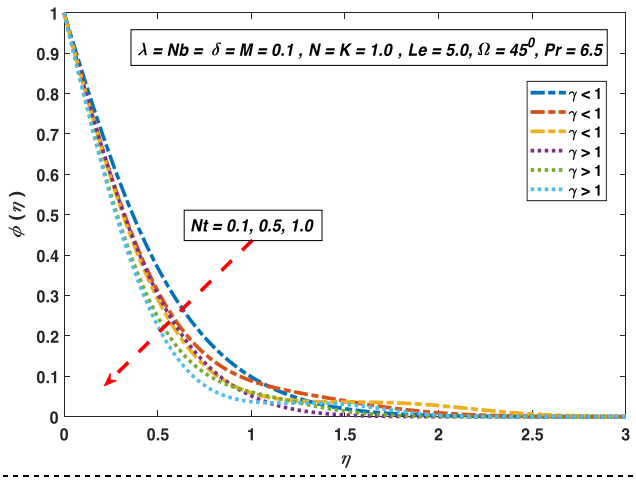

Fig. 10. Impacts of Thermophoresis parameter (Nt) on $\phi(\eta)$

An increase in Nb causes a decrease in boundary layer thickness, leading to a decrease in the concentration profile, as shown in Figure 11 for both cases of $\gamma < 1$ and $\gamma > 1$. Figure 12 shows a drop in the concentration outline as the Lewis number (Le) Increases.

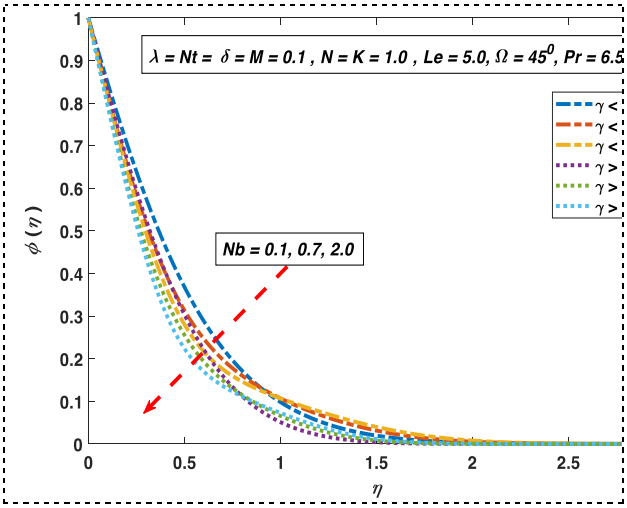

Fig. 11. Impacts of Brownian motion parameter (Nb) on $\phi(\eta)$

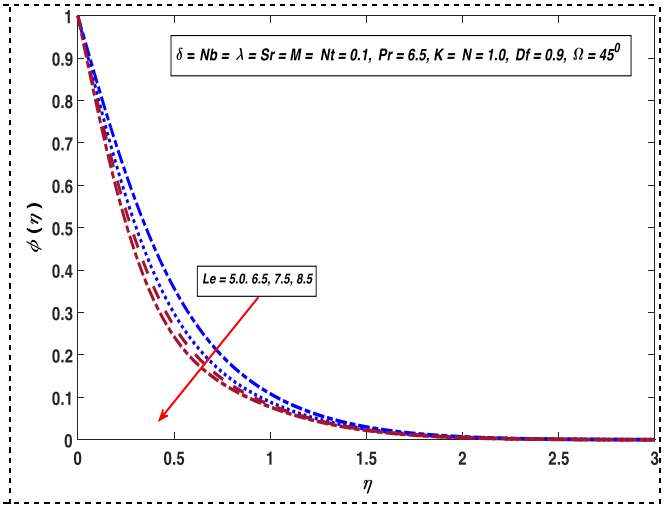

Fig. 12. Impacts of Lewis number (Le) on $\phi(\eta)$

4. Conclusions

This research investigates the stagnation point flow of a micropolar nanofluid over an exponentially stretching inclined surface, incorporating the Soret and Dufour effects. Moreover, thermal radiation effects are incorporated in the energy equation. Further, Soret and Dufour effects are also taken in account which help us to understand the fluid behavior in practical applications. For numerical simulation a well-known numerical technique called Keller box method is employed. The key findings of current research include:

- The value of $-\theta'(0)$ drops with the enhancement of Nb, Nt, M and Ω , but rises with the increase in λ, γ, and δ.
- $-\theta'(0)$ increases as values of S_r and D_f are increases.
- $C_{fx}(0)$ grows for higher values of D_f while, $-\phi'(0)$ and $C_{fx}(0)$ lowers for higher values of S_r
- An expansion in the inclination factor (Ω) results to an increase in $C_{fx}(0)$, but a decrease in $-\phi'(0)$ and $-\theta'(0)$.

Acknowledgement
The author extends his appreciation to the Arab Open University for funding this work through AOU research fund No. (AOURG-2025-048).

References

[1] Choi, S. U., and Eastman, J. A. "Enhancing Thermal Conductivity of Fluids with Nanoparticles." Argonne National Laboratory, 1995. ANL/MSD/CP-84938; CONF-951135-29. https://www.osti.gov/biblio/196525.

[2] Buongiorno, J. "Convective Transport in Nanofluids." *Journal of Heat and Mass Transfer* 128, no. 3 (2006): 240–250. https://doi.org/10.1115/1.2150834.

[3] Alhajaj, Z., Bayomy, A. M., Saghir, M. Z., and Rahman, M. M. "Flow of Nanofluid and Hybrid Fluid in Porous Channels: Experimental and Numerical Approach." *International Journal of Thermofluids* 1 (2020). https://doi.org/10.1016/j.ijft.2020.100016.

[4] Najib, N., Bachok, N., Dzulkifli, N. F., and Pop, I. "Numerical Results on Slip Effect over an Exponentially Stretching/Shrinking Cylinder." *Mathematics* 10, no. 7 (2022): 1114. https://doi.org/10.3390/math10071114.

[5] Najib, N., Bachok, N., Arifin, N. M., and Ali, F. M. "Stability Analysis of Stagnation-Point Flow in a Nanofluid over a Stretching/Shrinking Sheet with Second-Order Slip, Soret and Dufour Effects: A Revised Model." *Applied Sciences* 8, no. 4 (2018): 642. https://doi.org/10.3390/app8040642.
[6] Anuar, N. S., Bachok, N., Arifin, N. M., and Rosali, H. "Effect of Suction/Injection on Stagnation Point Flow of Hybrid Nanofluid over an Exponentially Shrinking Sheet with Stability Analysis." *CFD Letters* 11, no. 12 (2019): 21–33. https://akademiabaru.com/submit/index.php/cfdl/article/view/3199.
[7] Bouchireb, A., Khan, I., Kezzar, M., Alqahtani, S., Sari, M. R., Rafique, K., and Tabet, I. "MHD Flow of Hybrid Nanofluid Between Convergent/Divergent Channel by Using Daftardar-Jafari Method." *BioNanoScience* 14, no. 2 (2024): 1583–1600. https://doi.org/10.1007/s12668-024-01401-4.
[8] Ali, A. R., Rafique, K., Imtiaz, M., Jan, R., Alotaibi, H., and Mekawy, I. "Exploring Magnetic and Thermal Effects on MHD Bio-Viscosity Flow at the Lower Stagnation Point of a Solid Sphere Using Keller Box Technique." *Partial Differential Equations in Applied Mathematics* 9 (2024). https://doi.org/10.1016/j.padiff.2023.100601.
[9] Alotaibi, H., and Rafique, K. "Numerical Simulation of Nanofluid Flow Between Two Parallel Disks Using 3-Stage Lobatto III-A Formula." *Open Physics* 20, no. 1 (2022): 649–656. https://doi.org/10.1515/phys-2022-0059.
[10] Lemouedda, B., Kezzar, M., Rafique, K., Sari, M. R., Tabet, I., and Khan, I. "Ternary Nanoparticles Effect in Rotating Hydromagnetic Jeffery-Hamel Flow of Nanofluids." *Proceedings of the Institution of Mechanical Engineers, Part N: Journal of Nanomaterials, Nanoengineering and Nanosystems* (2024). https://doi.org/10.1177/23977914241261514.
[11] Rafique, K., Elkahlout, G., Rehman, A., and Kanwal, S. "Bio Convection Heat Transfer in Sisko Nanofluid Past a Stretching Cylinder with Soret and Dufour Effects." *Edelweiss Applied Science and Technology* 8, no. 6 (2024): 5236–5253. https://doi.org/10.55214/25768484.v8i6.3147.
[12] Al Faqih, F. M., Rafique, K., Aslam, S., and Swalmeh, M. Z. "Numerical Analysis on Stagnation Point Flow of Micropolar Nanofluid with Thermal Radiations over an Exponentially Stretching Surface." *WSEAS Transactions on Fluid Mechanics* 19 (2024): 40–48. https://doi.org/10.37394/232013.2024.19.4.
[13] Sakiadis, B. C. "Boundary Layer Behavior on Continuous Solid Surfaces: I. Boundary Layer Equations for Two-Dimensional and Axisymmetric Flow." *AIChE Journal* 7, no. 1 (1961): 26–28. https://doi.org/10.1002/aic.690070108.
[14] Daniel, Y. S., Aziz, Z. A., Ismail, Z., and Salah, F. "Impact of Thermal Radiation on Electrical MHD Flow of Nanofluid over Nonlinear Stretching Sheet with Variable Thickness." *Alexandria Engineering Journal* 57, no. 3 (2018): 2187–2197. https://doi.org/10.1016/j.aej.2017.07.007.
[15] Daniel, Y. S., Aziz, Z. A., Ismail, Z., and Salah, F. "Thermal Stratification Effects on MHD Radiative Flow of Nanofluid over Nonlinear Stretching Sheet with Variable Thickness." *Journal of Computational Design and Engineering* 5, no. 2 (2018): 232–242. https://doi.org/10.1016/j.jcde.2017.09.001.
[16] Warke, A. S., Ramesh, K., Mebarek-Oudina, F., and Abidi, A. "Numerical Investigation of the Stagnation Point Flow of Radiative Magnetomicropolar Liquid Past a Heated Porous Stretching Sheet." *Journal of Thermal Analysis and Calorimetry* 147 (2022): 6901–6912. https://doi.org/10.1007/s10973-021-10976-z.
[17] Rafique, K., Anwar, M. I., Misiran, M., and Asjad, M. I. "Energy and Mass Transport of Micropolar Nanofluid Flow over an Inclined Surface with Keller-Box Simulation." *Heat Transfer* 49, no. 8 (2020): 4592–4611. https://doi.org/10.1002/htj.21843.
[18] Uddin, I., Ullah, I., Raja, M. A. Z., Shoaib, M., Islam, S., Zobaer, M. S., and AlShahrani, S. "The Intelligent Networks for Double-Diffusion and MHD Analysis of Thin Film Flow over a Stretched Surface." *Scientific Reports* 11, no. 1 (2021): 1–20. https://doi.org/10.1038/s41598-021-97458-2.
[19] Rafique, K., Anwar, M. I., and Misiran, M. "Numerical Study on Micropolar Nanofluid Flow over an Inclined Surface by Means of Keller-Box." *Asian Journal of Probability and Statistics* 4 (2019): 1–21. https://doi.org/10.9734/ajpas/2019/v4i430122.
[20] Reddy, S. R. R., and Reddy, P. B. A. "Thermal Radiation Effect on Unsteady Three-Dimensional MHD Flow of Micropolar Fluid over a Horizontal Surface of a Parabola of Revolution." *Propulsion and Power Research* 11, no. 1 (2022): 129–142. https://doi.org/10.1016/j.jppr.2022.01.001.
[21] Reddy, S. R. R., and Anki Reddy, P. B. "Numerical Simulations of Unsteady 3D MHD Micropolar Fluid Flow over a Slendering Sheet." *Journal of Applied and Computational Mechanics* 7, no. 3 (2021): 1403–1412. https://doi.org/10.22055/jacm.2020.31062.1821.
[22] Rafique, K., Alghamd, S. M., and Alotaibi, H. "Energy and Mass Transfer Analysis of 3-D Boundary-Layer Flow over a Rotating Disk with Brownian Motion and Thermo-Phoretic Effects." *Thermal Science* 26, special issue 1 (2022): 107–115. https://doi.org/10.2298/TSCI22S1107R.
[23] Rafique, K., Anwar, M. I., Misiran, M., Khan, I., Alharbi, S. O., Thounthong, P., and Nisar, K. S. "Keller-Box Analysis of Buongiorno Model with Brownian and Thermophoretic Diffusion for Casson Nanofluid over an Inclined Surface." *Symmetry* 11, no. 11 (2019): 1370. https://doi.org/10.3390/sym11111370.

[24] Tarakaramu, N., Narayana, P. S., and Venkateswarlu, B. "Numerical Simulation of Variable Thermal Conductivity on 3D Flow of Nanofluid over a Stretching Sheet." *Nonlinear Engineering* 9, no. 1 (2020): 233–243. https://doi.org/10.1515/nleng-2020-0011.

[25] Hayat, T., Ullah, I., Muhammad, T., and Alsaedi, A. "Radiative Three-Dimensional Flow with Soret and Dufour Effects." *International Journal of Mechanical Sciences* 133 (2017): 829–837. https://doi.org/10.1016/j.ijmecsci.2017.09.015.

[26] Najib, N., and Bachok, N. "Boundary Layer Flow, Heat and Mass Transfer of Cu-Water Nanofluid over a Moving Plate with Soret and Dufour Effects: Stability Analysis." *Journal of Advanced Research in Fluid Mechanics and Thermal Sciences* 82, no. 1 (2021): 96–104. https://semarakilmu.com.my/journals/index.php/fluid_mechanics_thermal_sciences/article/view/7692.

[27] Sardar, H., Ahmad, L., Khan, M., and Alshomrani, A. S. "Investigation of Mixed Convection Flow of Carreau Nanofluid over a Wedge in the Presence of Soret and Dufour Effects." *International Journal of Heat and Mass Transfer* 137 (2019): 809–822. https://doi.org/10.1016/j.ijheatmasstransfer.2019.03.132.

[28] Khan, M. I., Hayat, T., Afzal, S., Khan, M. I., and Alsaedi, A. "Theoretical and Numerical Investigation of Carreau–Yasuda Fluid Flow Subject to Soret and Dufour Effects." *Computer Methods and Programs in Biomedicine* 186 (2020). https://doi.org/10.1016/j.cmpb.2019.105145.

[29] Qayyum, S., Hayat, T., Khan, M. I., Khan, M. I., and Alsaedi, A. "Optimization of Entropy Generation and Dissipative Nonlinear Radiative Von Karman's Swirling Flow with Soret and Dufour Effects." *Journal of Molecular Liquids* 262 (2018): 261–274. https://doi.org/10.1016/j.molliq.2018.04.010.

[30] Anwar, M. I., Ali, M., Rafique, K., and Shehzad, S. A. "Soret–Dufour and Radiative Aspects in Hydromagnetized Nanofluid Flow in Stratified Porous Medium." *SN Applied Sciences* 1 (2019): 1–15. https://doi.org/10.1007/s42452-019-1473-5.

[31] Rafique, K., Alqahtani, A. M., Ahmad, S., Alotaibi, H., Khan, I., and Singh, A. "Buongiorno Model of Micropolar Nanofluid with Surface Inclination and Soret Effect." *BioNanoScience* (2024): 1–11. https://doi.org/10.1007/s12668-024-01368-2.

[32] Ishak, A. "MHD Boundary Layer Flow Due to an Exponentially Stretching Sheet with Radiation Effect." *Sains Malaysiana* 40, no. 4 (2011): 391–395. https://myjurnal.mohe.gov.my/public/article-view.php?id=3254.

[33] Bidin, B., and Nazar, R. "Numerical Solution of the Boundary Layer Flow over an Exponentially Stretching Sheet with Thermal Radiation." *European Journal of Scientific Research* 33, no. 4 (2009): 710–717. https://www.researchgate.net/publication/229019114.

[34] Rafique, K., Anwar, M. I., Misiran, M., Khan, I., Seikh, A. H., Sherif, E. S. M., and Sooppy Nisar, K. "Keller-Box Simulation for the Buongiorno Mathematical Model of Micropolar Nanofluid Flow over a Nonlinear Inclined Surface." *Processes* 7, no. 12 (2019): 926. https://doi.org/10.3390/pr7120926.